Attitude motion of cylinder in variable electrostatic field near L1 libration point

Vladimir S. Aslanov[1]
Samara National Research University, 34, Moscovskoe shosse, Samara 443086, Russia

This paper explores the spatial attitude motion of an electrostatic cylindrical container (E-container) in a variable attracting electrostatic field. This field generated by the E-container and the orbiting spacecraft (orbiter) located at the L1 libration point of the Mars-Phobos system is used to capture the E-container by the orbiter in the Phobos Sample Return mission. Based on the Lagrange formalism and using the Euler angles, the equations of attitude motion of a cylindrical E-container are constructed in the framework of the circular restricted three-body problem with the addition of the electrostatic force and torque acting on the E-container. For modeling electrostatic force and torque acting on a cylindrical E-container, the Multi-Sphere Method is used, which was developed by Stevenson and Schaub. The influence of gravitational, centrifugal, and electrostatic moments on angular motion for different initial conditions has been studied both analytically analyzing the equations of attitude motion and numerical simulations. It is shown that the action of the above torques as the E-container approaches the orbiter causes the excitation of high-frequency nutation oscillations with large amplitudes. On the other hand, there are no natural and artificial factors of physical nature that could lead to damping of oscillations of large amplitude, and this fact corresponds to the obtained equations of attitude motion. And, the electrostatic torque is the greatest contributor to the oscillations with large amplitude. Hence, it is clear that the E-container must have a spherical current-conducting shell, in which case the electrostatic torque turns to zero.

Nomenclature

a	=	abscissa of the L_1 libration point, m
d	=	distance between Mars and Phobos, m
G	=	Newtonian gravitational constant, $6.67428 \cdot 10^{-11}$, $\mathrm{m}^3 \cdot s^{-2} \cdot kg^{-1}$
k_C	=	Coulomb's constant, $8.99 \cdot 10^9$ $N \cdot \mathrm{m}^2 \,/\, C^2$

[1] Head of Department, Professor, Theoretical Mechanics Department, 34, Moscovskoe Shosse, aslanov_ vs@mail.ru

m_1 = mass of Mars, kg

m_2 = mass of Phobos, kg

m_3 = mass of the E-container, kg

n = mean motion, sek^{-1}

λ_D = Debye length, m

μ = $m_2 / (m_1 + m_2)$

ε = coefficient of the orbiter voltage level control law

Φ = coefficient of the orbiter voltage level control law, kV

Φ_O = the voltage level of the orbiter, kV

Φ_C = the voltage level of the E-container, kV

Ω = angular spin velocity of the E-container about the symmetry axis, sek^{-1}

Subscripts

1 = Mars

2 = Phobos

3 = E-container

I. Introduction

Scientific missions to explore planets and their moons are of great research interest in studying their unknown origin and formation. In the past 50 years, this has concerned the study of the Moon, when samples return were repeatedly delivered to Earth by missions of the Soviet Union, the United States, and China. The Japan Aerospace Exploration Agency (JAXA) has implemented two unique missions Hayabusa and Hayabusa-2 to deliver samples return from the asteroids Itokawa and Ryugu, already in the 21st century [1-4]. In recent years, the study of Mars and its satellites Phobos and Deimos by means of return missions has become one of the fundamental problems of astronautics [5-15]. Returning samples from the planet and its moons provide an opportunity for new insights related to the planet's formation and configuration. In the Martian sample return missions, it has been proposed that a sample return container (SRC) is launched using a Mars Ascent Vehicle after samples are collected by the Mars 2020 rover [12]. However, rendezvous and docking of an orbiter to catch the SRC is a challenging and unsolved aspect of the current mission architecture. Also, rendezvous and docking in deep-space require autonomous navigation and control

capabilities. An Earth-based ground station in real-time cannot control a deep-space satellite. A solution to this problem of docking in deep-space the prospects of the SRC using electrostatic force were discussed in [5]. In this paper, the proposed method uses electrostatic interaction to retrieve a SRC launched from a planet by a small rocket. To safely perform rendezvous and docking in orbit, the possibility of rotational motion control for a cylindrical SRC was discussed. Papers [13, 14] explore the feasibility and benefits of the Phobos sample return delivery mission to a Phobos Sample Return to the orbiter using the electrostatic field artificially generated in proximity to the Mars–Phobos L1 libration point. The proposed method uses the electrostatic interaction to retrieve a SRC launched from Phobos. An artificial attractive electrostatic field is created by a charged container and a charged orbiter placed at the L1 point of libration. This field leads to the splitting of the unstable L1 libration point into two other unstable libration points and the formation of a stable L1 libration point [16]. The feasibility of the proposed retrieval system is discussed from the aspect of local space weather Debye length. The container's motion is studied, and the conditions of reaching the small given vicinity, the L1 point, are determined. The proposed mission's principal feasibility is demonstrated. The influence of the electrostatic charge level and the Debye length is studied on the container trajectory and the possibility of capturing the SRC. In addition, paper [14] proposes a control law of the electrostatic charge of the orbiter, which leads the electrostatic SRC in the vicinity of the L1 collinear libration point. In the final stage of the capture process, when the cylindrical container is to be fixed using a capture device of some kind. The success of this stage depends not least on the attitude motion of the container just before it is fixed, so it is necessary to know the angular velocities and orientation angles of the container at this stage, and therefore for the whole trajectory. In addition, if these angular velocities and orientation angles exceed the specified limits at the moment of container fixation, it is necessary to provide measures leading to reduction of angular motion parameters which exceeded the specified limits. A relatively small number of papers, e.g., [17-20], are devoted to study of angular motion of a rigid body under the action of gravitational and centrifugal forces and torques in the restricted three-body problem. It is worth noting that studies of the angular motion taking into account the action of an electrostatic torque have not yet been conducted.

And if electrostatic forces and torques are added to the classical restricted three-body problem, so such studies have not been conducted to date. It is well known that electrostatic forces are inversely proportional to the square of the distance between the charged bodies that generate these forces, then it becomes clear that the torque of these forces increases as the container approaches the orbiter and has a significant effect on the attitude motion of the container.

The purpose of the paper is to study of the attitude motion of the container under the action of gravitational, centrifugal and electrostatic forces and torques in the vicinity of the L1 libration point. This paper deals with an attitude motion of an electrostatic cylindrical container (E-container) in an attracting electrostatic field. For modeling

electrostatic force and torque acting on the E-container, known as the Multi-Sphere Method (MSM) is used, which was developed by Stevenson and Schaub. A cylinder is replaced by three spheres, the radii of which and the distance between the spheres are determined according to this method. It is well known that the magnitude of the electrostatic force, and hence the torque of this force, is inversely proportional to the square of the distance between the charged bodies. As the E-container approaches the orbiter at point L1, the electrostatic torque is going to have more and more influence on the attitude motion of the E-container. It makes it relevant to investigate the attitude motion of the cylindrical E-container in the restricted three-body problem, taking into account the electrostatic forces and torques.

The implementation of the purpose is carried out in the paper in four stages:

1) Formulation of assumptions that do not violate a physical essence of the problem
2) Calculation of forces and torques acting on an axisymmetric E-container in electrostatic and two gravitational fields in the rotating local-vertical-local-horizontal $Oxyz$ frame
3) Derivation of the equations of attitude motion of the axisymmetric E-container using the Lagrangian formalism and Euler angles
4) Performing simulation by numerical integration of the resulting equations of motion to identify features of the attitude motion.

II. Key Assumptions and Equations of Motion

A. Key Assumptions

We introduce acceptable assumptions that do not violate a physical essence of the study problem:

1. Mass of the E-container m_3 is significantly less than mass of any of the primaries (Mars-Phobos)

$$m_3 \ll m_2 < m_1 \tag{1}$$

2. The Phobos' orbit is circular. Although, in reality, this orbit has a small eccentricity ($e = 0.015$). In addition, the Martian gravity perturbations will not be taken into account, as the motion of the container within 10 meters of the L1 point will be investigated.
3. The Mars-Phobos L1 libration point is fixed in the Mars-Phobos system and the L1 point location is the fixed-point relative to the moon's surface.
4. In all considered cases, only in-plane motion of the center of mass of the E-container is studied.
5. On the contrary, the attitude motion of the E-container around its center of mass is considered as spatial defined by the Euler angles ψ , θ and φ (precession, nutation and rotation).
6. The E-container is an axisymmetric rigid body

$$J_x, J_y, J_z = J_x \tag{2}$$

where J_x, J_y, J_z are the axial moments of inertia of the container in the associated E-container $CXYZ$ frame (Fig. 1).

7. The height of the cylindrical E-container is much less than the distance the libration point L_1 and the center of mass of the E-container

$$h \ll R \tag{3}$$

where h is the height of the cylindrical E-container.

8. The Hill's sphere is located inside Debye sphere; as it appeared was accepted in [13, 14, 16]. Note that Debye length (radius of the Debye sphere) λ_D is an important parameter because the electrostatic field rapidly decreases beyond this length by the Debye shielding effect. However, the Debye length near the collinear libration points is usually unknown. Only approximate values of the Debye length for the Stickney crater, located on Phobos's surface directly under the L1 libration point at a distance of approximately 3.5 km, are given in the literature [21]. Depending on Mars local time, this parameter ranges from 13 to 47 m.
9. The solar radiation pressure [22, 23] is not considered.
10. In the electrostatic sense, the orbiter is modeled as spheres with radii R_1 and the E-container is modeled as three equivalent spheres, shown in Fig. 2, according to the Multi-Sphere Method which was developed by Stevenson and Schaub [24].

B. Forces and torques acting on the E-container

Consider the mass center of the E-container planar motion in the local-vertical-local-horizontal $Oxyz$ frame and the spatial motion around the mass center of an axisymmetric E-container ($J_x, J_y, J_z = J_x$) in the $CXYZ$ frame (Fig.1). The axes of the associated E-container $CXYZ$ frame are chosen so that at zero Euler angles, the axes of this frame are parallel to the corresponding axes of the local-vertical-local-horizontal $Oxyz$ frame. The frame $Oxyz$ rotates around the axis with a constant angular velocity $n = const$.

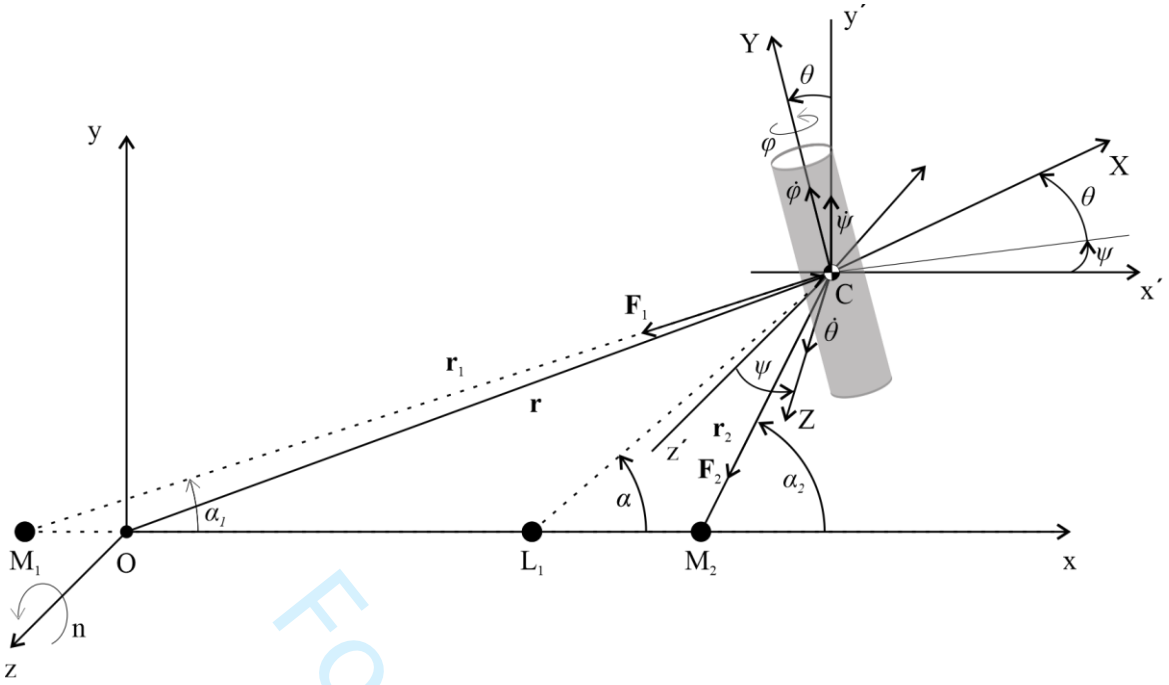

Fig. 1 The frame $Oxyz$ and $CXYZ$.

The gravitational forces $\mathbf{F}_1$ and $\mathbf{F}_2$ acting on the E-container from the two primaries are expressed in the frame $Oxyz$ as

$$\mathbf{F}_1 = -G\frac{m_1 m_3}{r_1^3}\mathbf{r}_1 \qquad (r_1 = \sqrt{(x+d\mu)^2 + y^2}) \tag{4}$$

$$\mathbf{F}_2 = -G\frac{m_2 m_3}{r_2^3}\mathbf{r}_2 \qquad (r_2 = \sqrt{(x-d(1-\mu))^2 + y^2}) \tag{5}$$

and the centrifugal force due to the rotation of the frame $Oxyz$ is

$$\mathbf{F}_{cf} = -m_3\,\mathbf{n}\times(\mathbf{n}\times\mathbf{r}) \qquad (r = \sqrt{x^2+y^2}) \tag{6}$$

$$\mathbf{r} = (x, y, 0) = (r\cos\alpha, r\sin\alpha, 0)^T, \quad \mathbf{n} = (0, 0, n)^T \tag{7}$$

where n is the mean motion, $(x, y, 0)$ are the coordinates of the E-container in the frame $Oxyz$.

The torques of the gravitational and centrifugal forces (4)-(6) relative to the mass center of the E-container are determined by the following expressions

$$\mathbf{L}_{\text{grav1}} = \int \boldsymbol{\rho}\times d\,\mathbf{F}_1 = -Gm_1\int \boldsymbol{\rho}\times\frac{(\mathbf{r}_1+\boldsymbol{\rho})}{\left[(\mathbf{r}_1+\boldsymbol{\rho})^2\right]^{3/2}}dm = -Gm_1\int\frac{\boldsymbol{\rho}\times\mathbf{r}_1}{\left[(\mathbf{r}_1+\boldsymbol{\rho})^2\right]^{3/2}}dm \tag{8}$$

$$\mathbf{L}_{\text{grav2}} = \int \boldsymbol{\rho}\times d\,\mathbf{F}_2 = -Gm_2\int \boldsymbol{\rho}\times\frac{(\mathbf{r}_2+\boldsymbol{\rho})}{\left[(\mathbf{r}_2+\boldsymbol{\rho})^2\right]^{3/2}}dm = -Gm_2\int\frac{\boldsymbol{\rho}\times\mathbf{r}_2}{\left[(\mathbf{r}_2+\boldsymbol{\rho})^2\right]^{3/2}}dm \tag{9}$$

$$\mathbf{L}_{cf} = \int \boldsymbol{\rho} \times d\,\mathbf{F}_{cf} = -\int \boldsymbol{\rho} \times \mathbf{n} \times (\mathbf{n} \times (\mathbf{r} + \boldsymbol{\rho}))dm \tag{10}$$

where the integrals (8)-(10) are taken over the entire volume of the E-container, $\boldsymbol{\rho} = (X, Y, Z)^T$ is radius vector of a mass element dm of the $CXYZ$ frame

$$\mathbf{r}_1 = (r_1 \cos\alpha_1, r_1 \sin\alpha_1, 0)^T,\ \mathbf{r}_2 = (r_2 \cos\alpha_2, r_2 \sin\alpha_2, 0)^T \tag{11}$$

$$\sin\alpha_1 = \frac{y}{\sqrt{(x+\mu d)^2 + y^2}}, \qquad \cos\alpha_1 = \frac{x+\mu d}{\sqrt{(x+\mu d)^2 + y^2}} \tag{12}$$

$$\sin\alpha_2 = \frac{y}{\sqrt{(x-(1-\mu)d)^2 + y^2}}, \quad \cos\alpha_2 = \frac{x-(1-\mu)d}{\sqrt{(x-(1-\mu)d)^2 + y^2}} \tag{13}$$

where $\mu = \dfrac{m_2}{m_1 + m_2}$, d is the distance between Mars and Phobos.

We introduce an additional frame $Cx'y'z'$ with axes parallel to the corresponding axes of the $Oxyz$ frame. The connection between the $Cx'y'z'$ and $CXYZ$ frames occurs through the three Euler angles ψ, θ and φ (precession, nutation and rotation). The rotation matrix from the $Cx'y'z'$ frame to the $CXYZ$ frame is

$$A = A_\varphi \cdot A_\theta \cdot A_\psi = \begin{bmatrix} \cos\varphi & 0 & -\sin\varphi \\ 0 & 1 & 0 \\ \sin\varphi & 0 & \cos\varphi \end{bmatrix} . \begin{bmatrix} \cos\theta & \sin\theta & 0 \\ -\sin\theta & \cos\theta & 0 \\ 0 & 0 & 1 \end{bmatrix} . \begin{bmatrix} \cos\psi & 0 & -\sin\psi \\ 0 & 1 & 0 \\ \sin\psi & 0 & \cos\psi \end{bmatrix} \tag{14}$$

Consider first the gravitational torque $\mathbf{L}_{\text{grav1}}$ (8). A Taylor series decomposition of the function $1/r_1^3$ with exclusion of an order of magnitude of the square $(\rho / r_1)^2$, allows to write

$$\frac{1}{\left[(\mathbf{r}_1 + \boldsymbol{\rho})^2\right]^{3/2}} = \frac{1}{r_1^3}\left(1 - \frac{3}{r_1^2}\boldsymbol{\rho} \cdot \mathbf{r}_1\right) \tag{15}$$

The center of the $CXYZ$ frame is in the mass center of the E-container, and therefore the following formulas can be written

$$\int (Y^2 - Z^2)dm = J_z - J_y \qquad \int (Z^2 - X^2)dm = J_x - J_z = 0 \qquad \int (Y^2 - X^2)dm = J_x - J_y \tag{16}$$

Taking into account the formulas (16) and using the transition matrix (14) from the $Oxyz$ frame to the $CXYZ$ frame the gravitational torque (8) for an axisymmetric E-container ($J_x = J_z$) is written as

$$\mathbf{L}_{\text{grav1}} = \frac{3Gm_1}{2r_1^3}(J_y - J_x)(\cos\psi\cos\alpha_1\sin\theta - \cos\theta\sin\alpha_1)$$
$$\left[-(\cos\theta\cos\psi\cos\alpha_1\sin\varphi + \cos\varphi\cos\alpha_1\sin\psi + \sin\theta\,\text{in}\,\varphi\sin\alpha_1)\mathbf{i} + \right.$$
$$\left.(\cos\alpha_1(\cos\theta\cos\varphi\cos\psi - \sin\varphi\sin\psi) + \cos\varphi\sin\theta\sin\alpha_1)\mathbf{k}\right] \quad (17)$$

where $\mathbf{i}, \mathbf{j}, \mathbf{k}$ are the Cartesian unit vectors of the $CXYZ$ frame.

By analogy with Eq. (17) the gravitational torque (9) can be written as

$$\mathbf{L}_{\text{grav2}} = \frac{3Gm_1}{2r_2^3}(J_x - J_y)(\cos\psi\cos\alpha_2\sin\theta - \cos\theta\sin\alpha_2)$$
$$\left[(\cos\theta\cos\psi\cos\alpha_2\sin\varphi + \cos\varphi\cos\alpha_2\sin\psi + \sin\theta\,\text{in}\,\varphi\sin\alpha_2)\mathbf{i} - \right.$$
$$\left.(\cos\alpha_2(\cos\theta\cos\varphi\cos\psi - \sin\varphi\sin\psi) + \cos\varphi\sin\theta\sin\alpha_2)\mathbf{k}\right] \quad (18)$$

In Eqs. (17) and (18), the angles α_1 and α_2 are defined by equations (12) and (13) .

In order to determine the centrifugal torque (10), it should be taken into account that point C is the mass center of the E-container and that the centrifugal moments of inertia are zero in the $CXYZ$ frame

$$\int XYdm = 0 \int XZdm = 0 \int YZdm = 0 \quad (19)$$

then the centrifugal torque (10) is

$$\mathbf{L}_{cf} = -\int \boldsymbol{\rho}\times\mathbf{n}\times(\mathbf{n}\times(\mathbf{r}+\boldsymbol{\rho}))dm = -\frac{n^2}{2}(J_x - J_y)\sin\theta\sin\psi\left[(\cos\varphi\cos\psi - \cos\theta\sin\psi\sin\varphi)\,\mathbf{i} + \right.$$
$$\left.(\sin\varphi\cos\psi + \cos\theta\sin\psi\cos\varphi)\mathbf{k}\right] \quad (20)$$

According to Ref. [24] the multi-sphere method (MSM) is a means to approximate the electrostatic interactions between conducting objects with generic geometries. Fig. 2 depicts a cylindrical E-container, modeled by three spheres A, C and B.

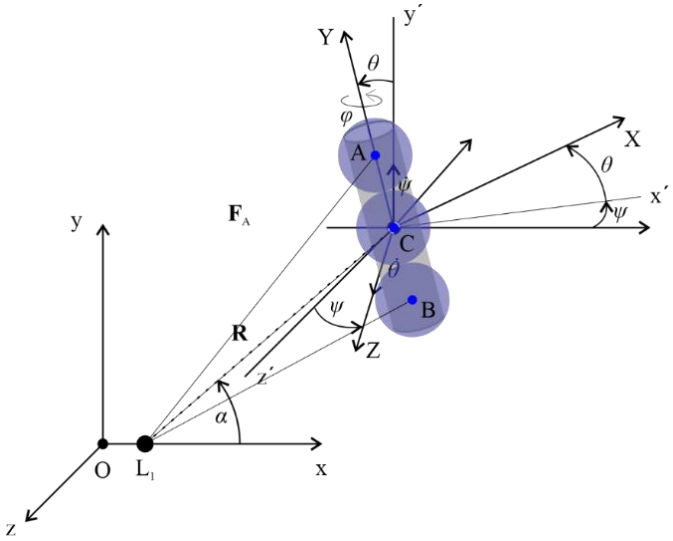

Fig. 2 The three-sphere model, frames, forces, coordinates.

The electrostatic forces (Coulomb forces) acting on the two outermost spheres A and B (Fig. 2) create the torque relative to the mass center of the E-container, which is equal to

$$\mathbf{L}_Q = (\mathbf{r}_{L_1} + \mathbf{l}) \times \mathbf{F}_A + (\mathbf{r}_{L_1} - \mathbf{l}) \times \mathbf{F}_B \tag{21}$$

where $\mathbf{F}_A$ and $\mathbf{F}_B$ are the electrostatic forces which Eq. (29) defines below, $\mathbf{l} = \overrightarrow{AC}(l,0,0)^T$ is the vector connecting the mass center of the E-container (point C) with the point A, $\mathbf{r}_{L_1}$ is the vector connecting the mass center of the E-container (point C) with the mass center of the Mars-Phobos system (point O) in the $Oxyz$ frame

$$\mathbf{r}_{L_1} = \mathbf{R} + \mathbf{L}_1 \tag{22}$$

$$\mathbf{R} = \overrightarrow{L_1 C} = (R\cos\alpha, R\sin\alpha, 0)^T, \ \mathbf{L}_1 = (a,0,0)^T \tag{23}$$

Where a is the abscissa of the L_1 libration point, $\mathbf{R}$ is the radius vector defining the position of the mass center C of the E-container relative to the L_1 libration point, $\mathbf{L}_1$ is the vector defining the position of the libration point L_1 in the frame $Oxyz$ (Fig.1). The Coulomb force between the spheres is dependent on the charge that each holds. The voltage on a given sphere is a result of both the charge on that sphere and the charges on its neighboring spheres (Fig. 2). Because voltages Φ_i are assigned to the objects, technically the charge q_i on each sphere depends on the voltage [24]. This relation is given in Eq. (1) Ref. [24], where R_i represents the radius of the sphere in question and $r_{i,j} = r_j - r_i$ is the center-to-center distance to each neighbor

$$\Phi_i = k_c \frac{q_i}{R_i} + \sum_{j=1, j\neq i}^{m} k_C \frac{q_j}{r_{i,j}} \tag{24}$$

These relations can be combined for each sphere to obtain the matrix equation

$$\begin{bmatrix} \Phi_O \\ \Phi_C \\ \Phi_C \\ \Phi_C \end{bmatrix} = k_C \left[C_M\right]^{-1} \begin{bmatrix} q_1 \\ q_A \\ q_C \\ q_B \end{bmatrix} \tag{25}$$

where Φ_O and Φ_C are the voltage levels of the orbiter and E-container,

$$\left[C_M\right]^{-1} = \begin{bmatrix} 1/R_1 & 1/r_A & 1/r_C & 1/r_B \\ 1/r_A & 1/R_{2,A} & 1/l & 1/2l \\ 1/r_b & 1/l & 1/R_{2,C} & 1/l \\ 1/r_c & 1/2l & 1/l & 1/R_{2,B} \end{bmatrix} \tag{26}$$

where R_1 is the radius of the orbiter, $R_{2,A}$, $R_{2,B}$, $R_{2,C}$ are radii of equivalent spheres according to the MSM (Fig. 2). The three-sphere MSM is applicable if the distance between the bodies (R) is assumed to be much greater than the given radii [24]

$$R \gg R_1, R_{2,A}, R_{2,B}, R_{2,C} \tag{27}$$

By inverting $\left[C_M\right]^{-1}$, the charge on each sphere is determined at any instance of time. The charge redistribution and interaction with the space environment are assumed to be orders of magnitude faster than the spacecraft motion. The total electrostatic force is then given by the summations [24]

$$\mathbf{F}_{Container} = -\mathbf{F}_{Orbiter} = k_C \left|q_1\right| \sum_{i=A}^{C} \frac{q_i}{r_i^3} \mathbf{r}_i \tag{28}$$

and for each of the three spheres of the E-container

$$\mathbf{F}_i = k_C \frac{\left|q_1\right| q_i}{r_i^3} \mathbf{r}_i, \qquad (i = A, B, C) \tag{29}$$

$$\mathbf{r}_A = \mathbf{R} + A^T \cdot \begin{bmatrix} 0 \\ l \\ 0 \end{bmatrix}, \qquad \mathbf{r}_B = \mathbf{R} + A^T \cdot \begin{bmatrix} 0 \\ -l \\ 0 \end{bmatrix} \tag{30}$$

where l is the distance between the points C and A (or B).

The motion of the E-container is considered in a variable attracting field, when the voltage level of the orbiter changes according to the control law [14],

$$\Phi_O = \Phi(1 + \varepsilon \frac{\dot{R}}{nR}) \tag{31}$$

where Φ and ε are the coefficients of the control law. Taking into account Eq. (31) the matrix equation (25) is written as

$$\begin{bmatrix} -\Phi(1 + \varepsilon \dfrac{\dot{R}}{nR}) \\ \Phi_C \\ \Phi_C \\ \Phi_C \end{bmatrix} = k_C \left[C_M\right]^{-1} \begin{bmatrix} q_1 \\ q_A \\ q_C \\ q_B \end{bmatrix} \tag{32}$$

The equation for the electrostatic torque (21) is expanded into a power series in powers of the parameter

$$\lambda = \frac{l}{R}$$

which according to the condition (3) is always less than 1. Then if in this series one neglects the terms of the order of 2 and higher, the electrostatic torque acting on the E-container from the side of the orbiter in the $CXYZ$ frame can be approximately written as

$$\mathbf{L}_Q = \frac{k_Q}{R^2}\big[-(\sin\alpha\sin\theta\sin\varphi + \cos\alpha(\cos\theta\cos\psi\sin\varphi + \cos\varphi\sin\psi)), 0,$$

$$(\cos\varphi\sin\alpha\sin\theta + \cos\alpha(\cos\theta\cos\varphi\cos\psi - \sin\varphi\,\mathrm{in}\,\psi))\big] \tag{33}$$

where

$$k_Q = \frac{\Phi_O\Phi_C}{16k_C}\frac{l^2R_1(4lR_{2,A} - 3lR_{2,C} + 4R_{2,A}R_{2,C})}{R_{2,A}R_{2,C}} \tag{34}$$

C. Planar motion equations of the E-container center of mass in polar coordinates

By virtue of assumption (3) for modeling the E-container center of mass motion, one can suppose that the electrostatic forces (29) are directed along the vector $\mathbf{r}_C$, then the total Coulomb force vector is expressed as

$$\mathbf{F}_Q = \sum_{i=A,B,C}\mathbf{F}_i = \sum_{i=A,B,C} k_C\frac{|q_1|q_i}{r_i^3}\mathbf{r}_i \approx \frac{k_c|q_1|\sum\limits_{i=A,B,C} q_i}{R^2}\frac{\mathbf{r}_C}{R} = F_Q\frac{\mathbf{R}}{R} \qquad [\,\mathbf{R} = \mathbf{r}_C = \overrightarrow{L_1C} = (R\cos\alpha, R\sin\alpha, 0)^T\,] \tag{35}$$

Taking into account Eqs. (29) - (32) the magnitude of the total Coulomb force is

$$F_Q = -\frac{7lR_1\Phi(1 + \varepsilon\frac{\dot{R}}{nR})(R\Phi_C + R_1\Phi(1 + \varepsilon\frac{\dot{R}}{nR}))}{4k_CR^3} \tag{36}$$

Let us now consider the equations of the E-body planar motion in the Local-Vertical-Local-Horizontal frame Oxy within the scope of the classical restricted three-body problem [25, 26]

$$\ddot{x} = \frac{\partial W}{\partial x} + n^2 x + 2n\dot{y} - \frac{F_Q}{m_3}\frac{x-a}{R} \tag{37}$$

$$\ddot{y} = \frac{\partial W}{\partial y} + n^2 y - 2n\dot{x} - \frac{F_Q}{m_3}\frac{y}{R} \tag{38}$$

where m_3 is of the E-container mass

$$W(x,y) = G\left(\frac{m_1}{\sqrt{(x+d\mu)^2 + y^2}} + \frac{m_2}{\sqrt{(x-d(1-\mu))^2 + y^2}}\right) \tag{39}$$

Thus, Eqs. (37) and (38) describe the flight of the E-body under the action of the attractive electrostatic force (36) and the gravitational influence of the uniformly rotating planet-moon system. Since we study the motion of the E-body relative to the orbiter, which is in the L_i libration point $i = 1,2,3$, it makes sense to pass from the frame Oxy to the frame L_iXY by changing the variables (Fig. 1). Position of the E-body M_3 relative to the L_i libration points in a polar reference frame R,α is defined by substituting the variables

$$x = a + R\cos\alpha, \;\; y = R\sin\alpha \tag{40}$$

where a is the abscissa of the L_1 libration point. Eqs. (37) and (38) in the polar reference frame (Fig. 1) are written as

$$\ddot{R} = \frac{\partial U}{\partial R} + R(n+\dot{\alpha})^2 - \frac{F_Q}{m_3} \tag{41}$$

$$\ddot{\alpha} = \frac{\partial U}{\partial \alpha} - 2\frac{\dot{R}}{R}(n+\dot{\alpha}) \tag{42}$$

where the potential is

$$U = G\left(\frac{m_1}{r_1} + \frac{m_2}{r_2}\right) + \frac{1}{2}(nr)^2 \tag{43}$$

where the distance between the mass center of the primaries and the E-body is

$$r = \sqrt{a^2 + R^2 + 2aR\cos\alpha} \tag{44}$$

the distance between the primaries 1, 2 and the E-body

$$r_1 = \sqrt{R^2 + 2Ra_1\cos\alpha + a_1^2}\,, \qquad r_2 = \sqrt{R^2 - 2Ra_2\cos\alpha + a_2^2} \tag{45}$$

where

$$a_1 = a + d\mu\,,\ a_2 = d(1-\mu) - a \tag{46}$$

D. Lagrange equations of attitude motion equations of the E-container

We use the Lagrangian formalism to write the spatial attitude motion equations of the axisymmetric E-container

$$\frac{d}{dt}\frac{\partial T}{\partial \dot{s}} - \frac{\partial T}{\partial s} = L\,,\quad (i = 1,2,3) \tag{47}$$

where T is the kinetic energy of the attitude motion, $L = (L_\psi, L_\theta, L_\varphi)$ is the generalized forces, $s = (\psi, \theta, \varphi)$ are the generalized coordinates vector (the Euler angles: precession, nutation and rotation). The generalized forces $L = (L_\psi, L_\theta, L_\varphi)$ are the projections of vectors of gravitational, centrifugal and electrostatic torques on the Euler rotation axes

$$\mathbf{L} = \mathbf{L}_{\text{grav1}} + \mathbf{L}_{\text{grav2}} + \mathbf{L}_{cf} + \mathbf{L}_Q \tag{48}$$

The kinetic energy of the attitude motion is

$$T = \frac{J_x}{2}(\omega_x^{\,2} + \omega_z^{\,2}) + \frac{J_y}{2}\omega_y^{\,2} \tag{49}$$

where $\boldsymbol{\omega} = (\omega_x, \omega_y, \omega_z)$ is the angular velocity vector of the E-container in the $CXYZ$ frame (Fig. 1)

$$\omega_x = \dot{\psi}\sin\theta\cos\varphi - \dot{\theta}\sin\varphi \tag{50}$$

$$\omega_y = \dot{\psi}\cos\theta + \dot{\varphi} \tag{51}$$

$$\omega_z = \dot{\psi}\sin\theta\sin\varphi + \dot{\theta}\cos\varphi \tag{52}$$

Given that the projection of the total torque (48) on the CY coordinate axes is zero, so for an axisymmetric E-container ($J_x = J_z$) the angular velocity about the symmetry axis is constant, i.e.

$$\omega_y = \dot{\psi}\cos\theta + \dot{\varphi} = \Omega = const \tag{53}$$

where Ω - angular spin velocity of the E-container about the symmetry axis. Finally, based on Eqs. (17), (18), (20), (33), (49)-(53) the spatial attitude motion equations (47) are written as

$$\begin{aligned} J_x\ddot{\psi} = (J_x - J_y)\Bigg[&\frac{3Gm_1}{r_1^5}(a_1 + R\cos\alpha)(a_1\cos\psi + R(\cos\alpha\cos\psi - \cot\theta\sin\alpha))\sin\psi + \\ &\frac{3Gm_2}{r_2^5}(-a_2 + R\cos\alpha)(-a_2\cos\psi + R(\cos\alpha\cos\psi - \cot\theta\sin\alpha))\sin\psi - \\ &n^2\sin\psi\cos\psi\Bigg] + \dot{\theta}(J_y\Omega - 2J_x\dot{\psi}\cos\theta)\csc\theta - \frac{k_Q\cos\alpha\csc\theta\sin\psi}{R^2} \end{aligned} \tag{54}$$

$$J_x\ddot{\theta} = (J_x - J_y)\Bigg[-\frac{3Gm_1}{r_1^5}(a_1\sin\theta\cos\psi + R(-\sin\alpha\cos\theta + \cos\alpha\sin\theta\cos\psi))$$

$$(a_1\cos\theta\cos\psi + R(\cos\alpha\cos\theta\cos\psi + \sin\alpha\sin\theta)) -$$

$$\frac{3Gm_2}{r_2^5}(-a_2\sin\theta\cos\psi + R(-\sin\alpha\cos\theta + \cos\alpha\sin\theta\cos\psi))$$

$$(-a_2\cos\theta\cos\psi + R(\cos\alpha\cos\theta\cos\psi + \sin\alpha\sin\theta)) - n^2\sin\theta\cos\theta(\sin\psi)^2\Big] +$$

$$\dot{\psi}(J_x\dot{\psi}\cos\theta - J_y\Omega)\sin\theta + \frac{k_Q(\cos\alpha\cos\theta\cos\psi + \sin\alpha\sin\theta)}{R^2} \tag{55}$$

where

$$k_Q = \Phi\Phi_C(1+\varepsilon\frac{\dot{R}}{Rn})\frac{l^2R_1(4lR_{2,A} - 3lR_{2,C} + 4R_{2,A}R_{2,C})}{16k_CR_{2,A}R_{2,C}} \tag{56}$$

Note that if the electrostatic torque in Eqs. (54) and (55) is excluded ($k_Q = 0$), we obtain very simple equations of angular motion of an axisymmetric body in the Euler angle for the circular restricted three-body problem.

III. Numerical simulation

This section examines the influence of the angular spin velocity Ω, initial conditions, moments of inertia and voltages levels on the attitude motion of the cylindrical E-container near the L1 point of libration.

A. Basic simulation case

As can be seen from Eqs. (41) and (42), due to the assumptions (3), the motion of the mass center of the cylindrical E-container does not depend on its attitude motion, so these equations can be considered separately from the Eqs. (54) and (55). The artificial attractive electrostatic field created by the static charges of the E-container and the orbiter located at the L1 unstable libration point splits into two unstable L6 and L7 libration points, and itself becomes stable [13] as shown in Fig.3. In this case the motion of the E-container is considered inside the E-Hill's sphere [14], which is located between the L6 and L7 Lagrangian points. This motion corresponds to the new Jacobi integral [13]

$$J(R,\alpha) = 2G(\frac{m_1}{r_1} + \frac{m_2}{r_2}) - 2\frac{\mathrm{K}}{m_3R} + (nr)^2 - (\dot{R}^2 + R^2\dot{\alpha}^2) = const \tag{57}$$

where r, r_1 and r_2 are defined by the Eqs. (44)-(45), $\mathrm{K} = 7lR_1\Phi\Phi_C / (4k_C)$.

However, it is necessary to make one comment about the above equation, which is true for a constant electrostatic field, but in our case we have a variable field, so strictly speaking the equation (57) corresponds only to a constant orbiter voltage level.

For the numerical simulation of the E-container motion, consider as an example the cylinder presented in the paper [27]. The cylinder, constructed with a conducting surface, has a 15 cm diameter and a 45 cm length. The orbiter appears as a 2 meter radius sphere ($R_1 = 2\,m$). The voltage level of the E-container and the coefficients of the control law of the orbiter voltage level (31) are taken as follow

$$\Phi_C = 10\,kV \qquad \Phi = 20\,kV \qquad \varepsilon = 1 \tag{58}$$

Fig. 3 shows the two trajectories of the E-container that start at the points A and B, as the result of numerical integration of Eqs. (41) and (42) under the following initial conditions

point A: $$R_0 = 45.0\,m\,,\ \dot{R}_0 = -0.001\,m/s\,,\ \alpha_0 = 0\,,\ \dot{\alpha}_0 = 0 \tag{59}$$

point B: $$R_0 = 22.5\,m\,,\ \dot{R}_0 = -0.001\,m/s\,,\ \alpha_0 = \frac{\pi}{2}\,,\ \dot{\alpha}_0 = 0 \tag{60}$$

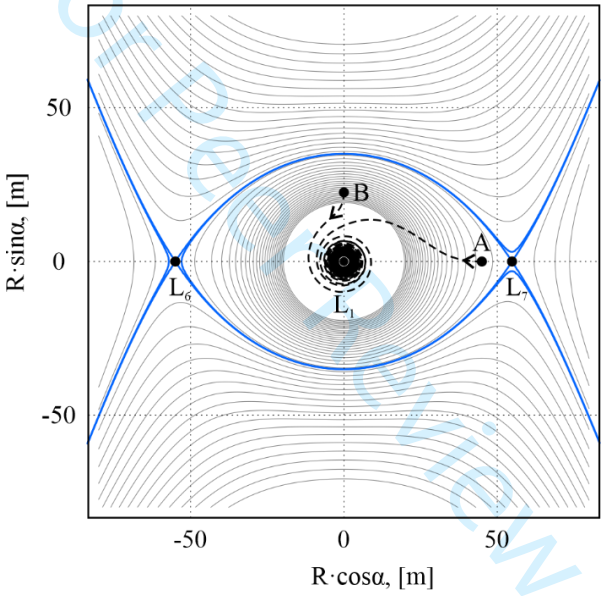

Fig. 3 The E-container trajectories for the initial conditions (59) and (60).

For the simulation of attitude motion, the cylinder parameters are given in Table 1 [27].

Table 1 Parameters of the cylinder E-container

Parameter	Value	Unit	Description
m_3	0.1821	kg	mass
J_x	0.00330	$kg \cdot m^2$	transverse moment of inertia
J_y	0.00205	$kg \cdot m^2$	longitudinal moment of inertia
l	0.17353	m	MSM parameters
$R_{2,A}$, $R_{2,B}$	0.088634	m	MSM parameters
$R_{2,C}$	0.097664	m	MSM parameters

Figs. 4a and 5a depict the oscillations of the E-container when, at the initial moment, its longitudinal axis is parallel to the axis Ox and the angular spin velocity is

$$\Omega = 1\,sek^{-1} \tag{61}$$

The initial conditions for numerical integration of Eqs. (54) and (55) are as follows

$$\theta_0 = \frac{\pi}{2}, \dot{\theta}_0 = 1.0\,rad\,/\,\sec, \psi_0 = 0, \dot{\psi}_0 = 0 \tag{62}$$

Numerical integration of Eqs. (41), (42), (54) and (55) continues until the E-collector reaches the orbiter surface ($R_f = R_1 = 2\,m$). Fig. 4 and Fig. 5 correspond to the start points A (59) and B (60), respectively.

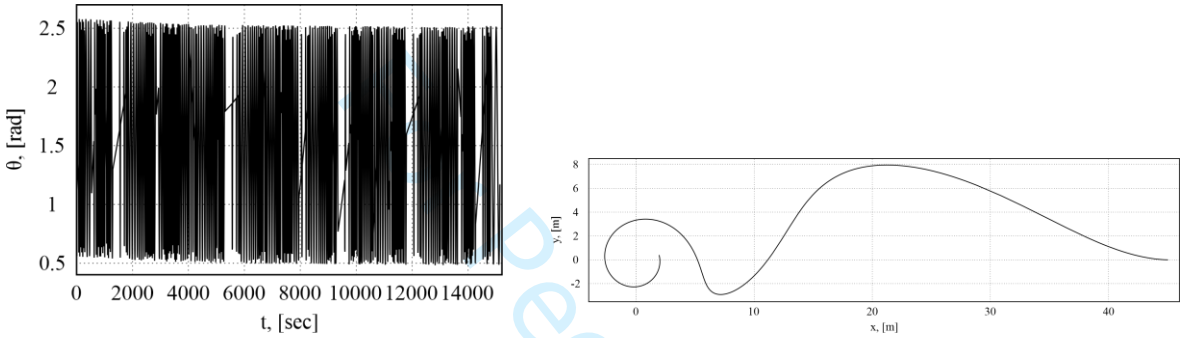

Fig. 4 Time history of the nutation angle $\theta(t)$ and the corresponding trajectory of the E-container $y(x)$ for the initial conditions (59), (62) and the angular spin velocity (61).

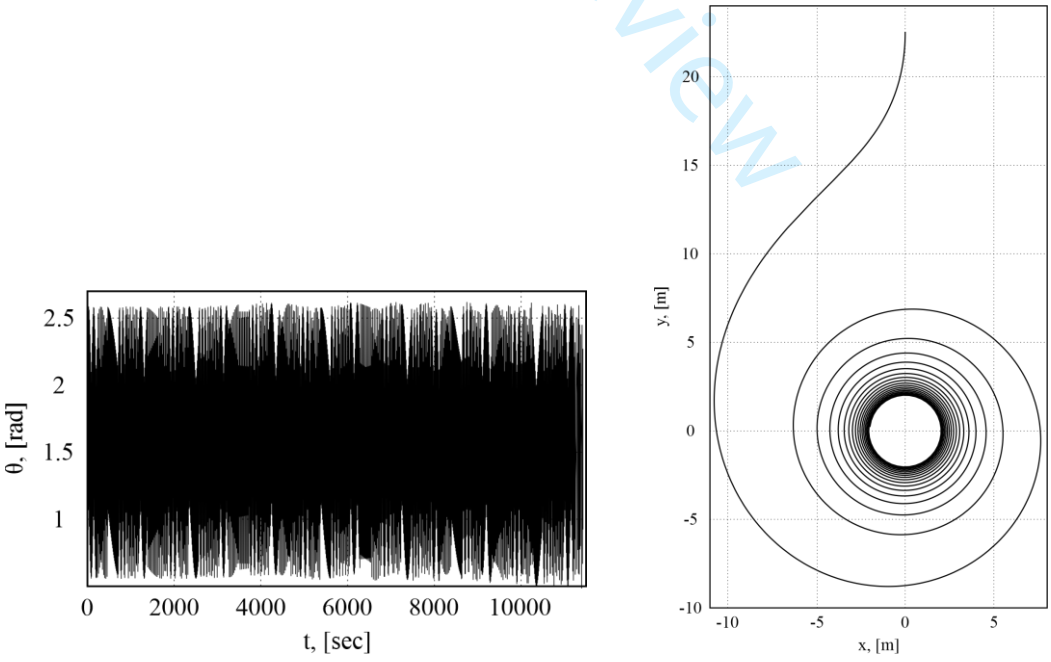

Fig. 5 Time history of the nutation angle $\theta(t)$ and the corresponding trajectory of the E-container $y(x)$ for the initial conditions (60), (62) and the angular spin velocity (61).

The base case (Fig. 5) will be defined by Table 1, the voltage levels (58), the angular spin velocity (61) and the initial conditions (60), (62). For this case the time history of the level voltage of the orbiter, which implements the law of control of the mass center of the E-container is shown in Fig. 6.

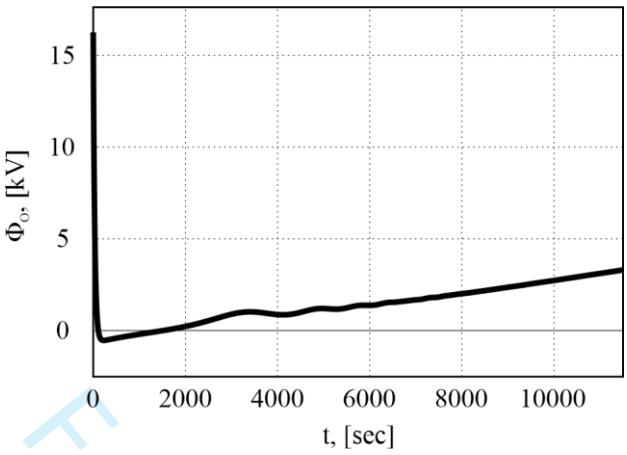

Fig. 6 Time history of the orbiter voltage level (31) **for the initial conditions (60), (62) and the angular spin velocity (61).**

The nutational motion of the E-container, which can be defined as tumbling, depends according to the Eq. (55) on the corresponding projections of gravitational $L_{grav,\theta}$, centrifugal $L_{cf,\theta}$ and electrostatic $L_{Q,\theta}$ torques, as follows

$$L_{grav,\theta} = 3G(J_x - J_y)[-\frac{m_1}{r_1^5}(a_1 \sin\theta\cos\psi + R(-\sin\alpha\cos\theta + \cos\alpha\sin\theta\cos\psi))$$

$$(a_1\cos\theta\cos\psi + R(\cos\alpha\cos\theta\cos\psi + \sin\alpha\sin\theta)) -$$

$$\frac{m_2}{r_2^5}(-a_2\sin\theta\cos\psi + R(-\sin\alpha\cos\theta + \cos\alpha\sin\theta\cos\psi))$$

$$(-a_2\cos\theta\cos\psi + R(\cos\alpha\cos\theta\cos\psi + \sin\alpha\sin\theta))] \quad (63)$$

$$L_{cf,\theta} = -(J_x - J_y)n^2\sin\theta\cos\theta(\sin\psi)^2 \quad (64)$$

$$L_{Q,\theta} = \frac{k_Q(\cos\alpha\cos\theta\cos\psi + \sin\alpha\sin\theta)}{R^2} \quad (65)$$

To examine the influence of the gravitational, centrifugal and electrostatic torques on the attitude motion of the E-container for the base scenario below are the time histories of these torques in Fig. 7. These illustrations give an idea of how these different torques compare to each other in magnitude, and answer the question: can the gravitational and centrifugal torques be neglected compared to the electrostatic torque? It appears that the electrostatic torque exceeds the gravitational and centrifugal torques by 4-5 orders of magnitude. From this it is clear that in the area bounded by a Debye sphere with center at the L1 libration point, where Coulomb's law applies, only the electrostatic torque can

be taken into account in the study of attitude motion of the E-container.

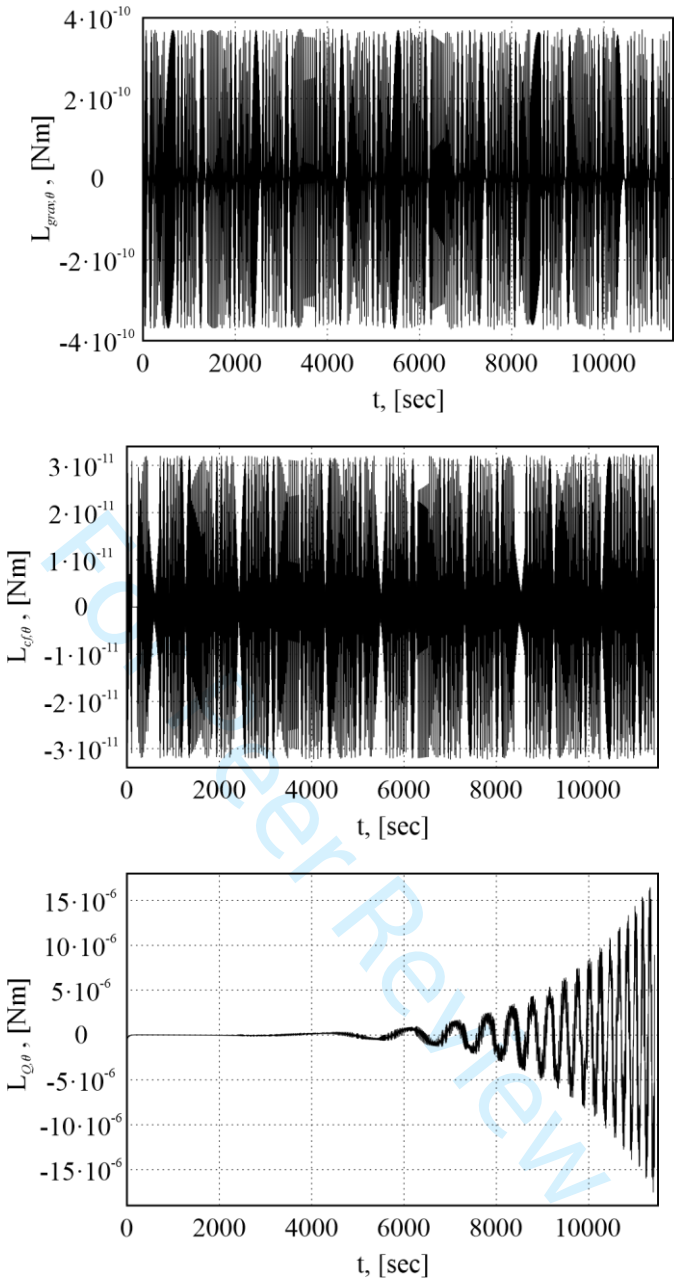

Fig. 7 Time history of the projections of gravitational $L_{grav,\theta}$, centrifugal $L_{cf,\theta}$ and electrostatic $L_{Q,\theta}$ torques for the initial conditions (60), (62) and the angular spin velocity (61).

Next, various parameters of the E-collector-orbiter system and the initial conditions of E-collector motion relatively to the base scenario will be varied.

B. Influence of the voltage level

Figs. 8-9 show the time history of the nutation angle and the trajectory of the E-container, for the cases when the E-container and the orbiter voltage level are changed compared with the basic values (58). In the first case, the E-

collector voltage level is doubled (Fig. 8) and in the second case, the orbiter voltage level is halved (Fig. 9)

Fig. 8: $\Phi_C = 20\,kV \qquad \Phi = 20\,kV$ (66)

Fig. 9: $\Phi_C = 10\,kV \qquad \Phi = 10\,kV$ (67)

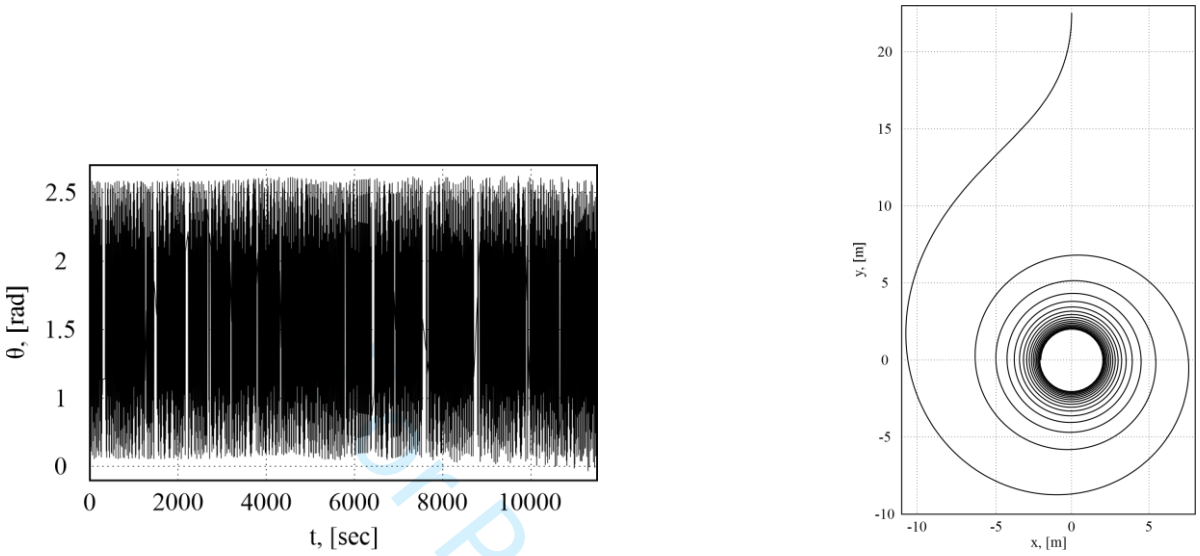

Fig. 8 Time history of the nutation angle $\theta(t)$ and the corresponding trajectory of the E-container $y(x)$ for the initial conditions (60), (62), the angular spin velocity (61) and the voltage level of the E-container and the orbiter (66).

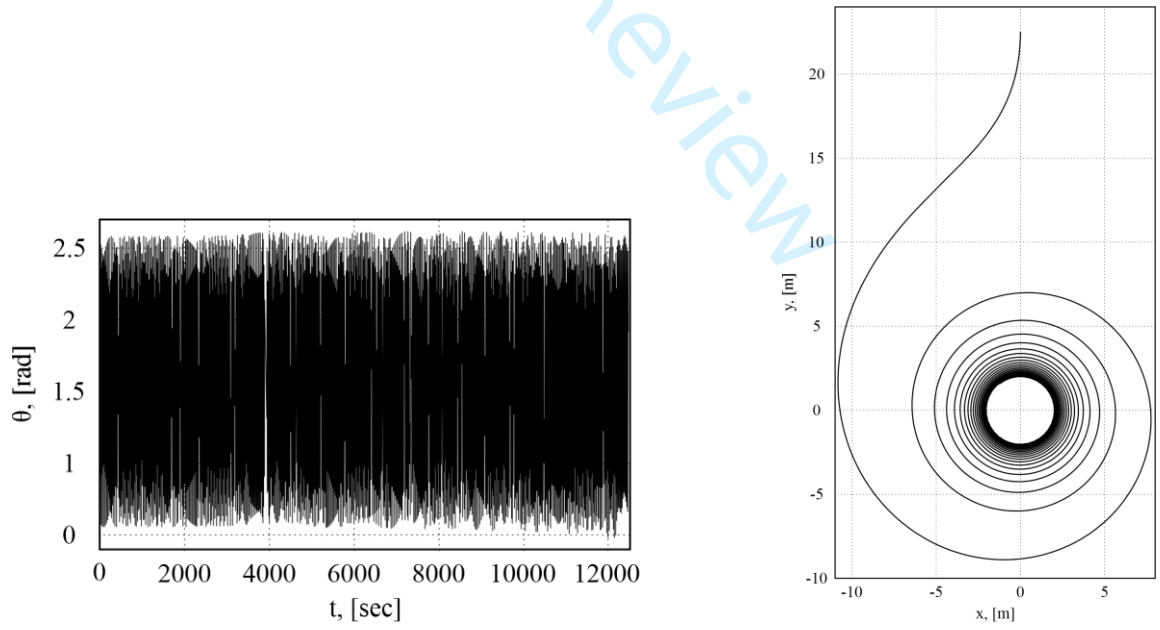

Fig. 9 Time history of the nutation angle $\theta(t)$ and the corresponding trajectory of the E-container $y(x)$ for the initial conditions (60), (62), the angular spin velocity (61) and the voltage level of the E-container and the orbiter (67).

The analysis of Figs. 5. 8 and 9 leads to the conclusion that the level of voltages insignificantly influences the attitude motion of the E-container. At the same time, it should be taken into account that the greater the product of the orbiter and E-container voltage level, the greater the area of capture of the E-container by the electrostatic field and the Hill sphere with the center in the L1 point libration is larger [14, 15].

C. Influence of the initial conditions of attitude motion

The initial conditions for numerical integration of Eqs. (54) and (55) in the base scenario were given by conditions (62). Here we consider two cases, when at the initial moment the E-container does not rotate (Fig. 10)

$$\theta_0 = \frac{\pi}{2}, \dot{\theta}_0 = 0, \psi_0 = 0, \dot{\psi}_0 = 0 \tag{68}$$

and when it has a greater angular velocity of nutation (Fig. 11) than in the base case (62)

$$\theta_0 = \frac{\pi}{2}, \dot{\theta}_0 = 2.0\, rad/\sec, \psi_0 = 0, \dot{\psi}_0 = 0 \tag{69}$$

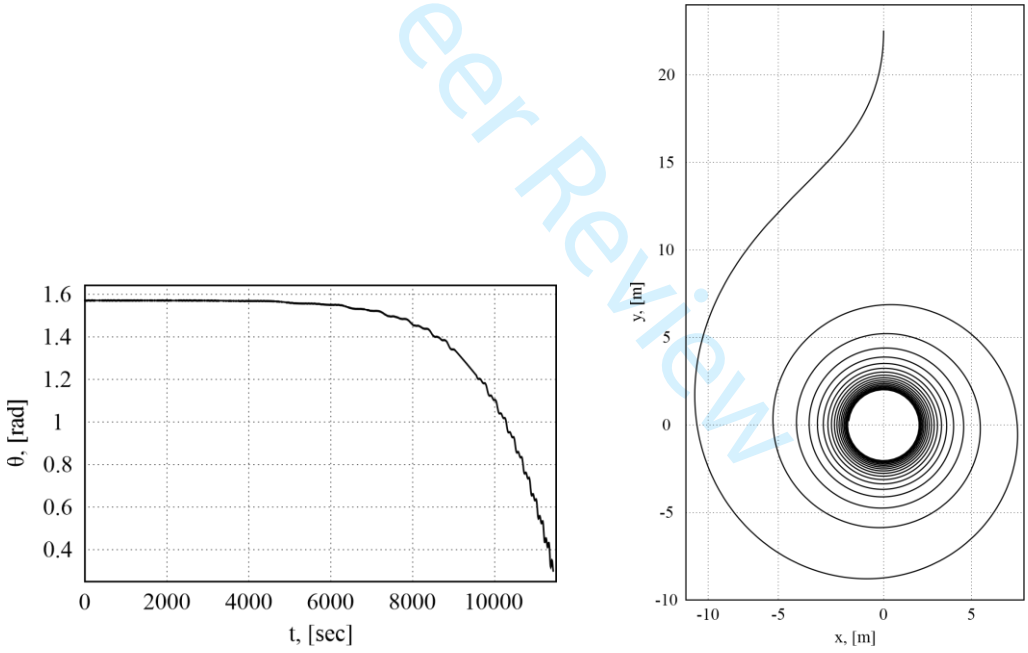

Fig. 10 Time history of the nutation angle $\theta(t)$ and the corresponding trajectory of the E-container $y(x)$ for the initial conditions (60), (68), the angular spin velocity (61).

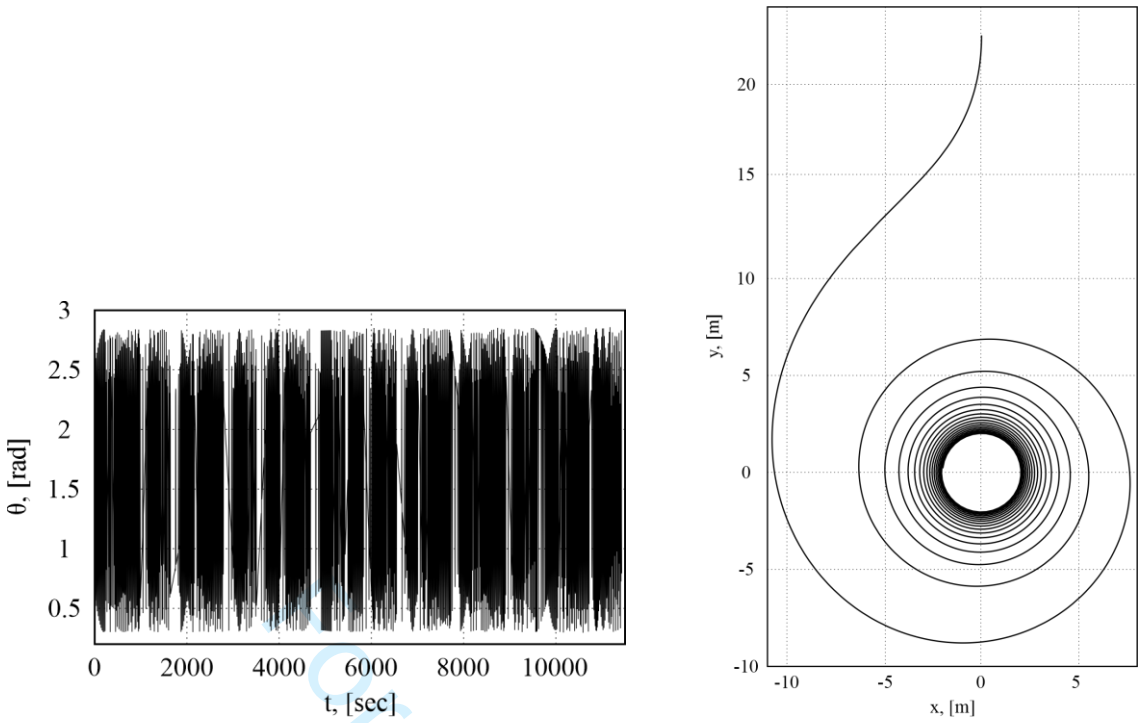

Fig. 11 Time history of the nutation angle $\theta(t)$ and the corresponding trajectory of the E-container $y(x)$ for the initial conditions (60), (69), the angular spin velocity (61).

Figs. 5, 10, and 11 show that the greater the initial time derivative of the nutation angle, the greater the amplitude of the E-container's nutation oscillations, and the oscillation amplitude does not decrease due to the absence of dissipative forces.

D. Influence of the angular spin velocity

If the angular spin velocity is increased by a factor of 10 compared to the base scenario (61), i.e.

$$\Omega = 10 sek^{-1} \tag{70}$$

then this leads to a significant decrease of the amplitude of nutation oscillations as shown in Fig. 12.

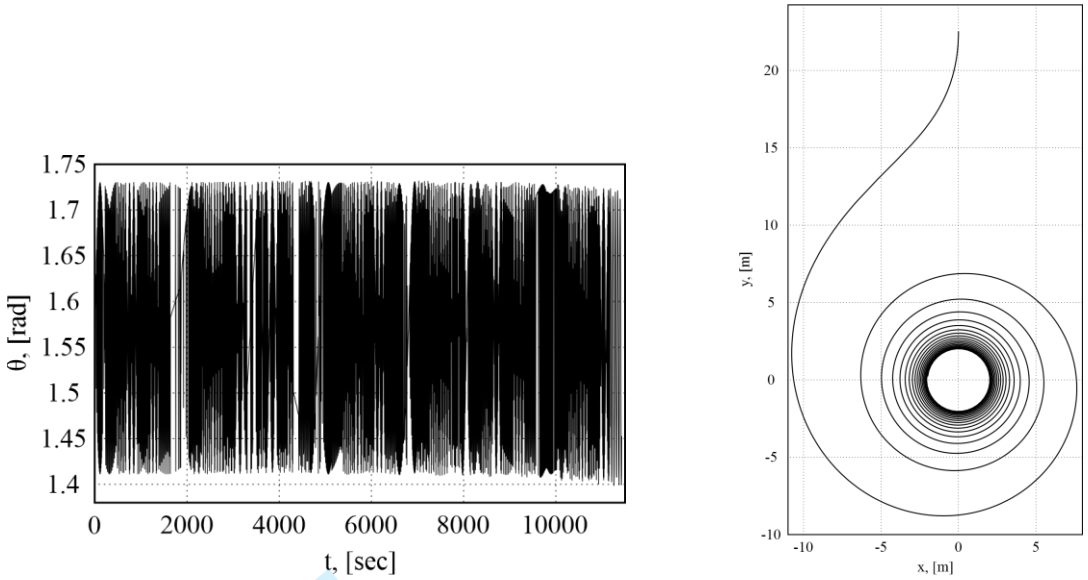

Fig. 12 Time history of the nutation angle $\theta(t)$ and the corresponding trajectory of the E-container $y(x)$ for the initial conditions (60), (62) and the angular spin velocity (70).

E. Influence of the moments of inertia and masses of the E-container

Fig. 13 shows the time history of the nutation angle $\theta(t)$ for the mass and moment of inertia of the E-container halved

$$m_3 = 0.0911\,kg, J_x = 0.00165\,kg\cdot m^2, J_y = 0.001025\,kg\cdot m^2 \tag{71}$$

compared to the corresponding data in Table 1. The initial angular spin velocity as for the previous case (Fig. 12) is defined from (70).

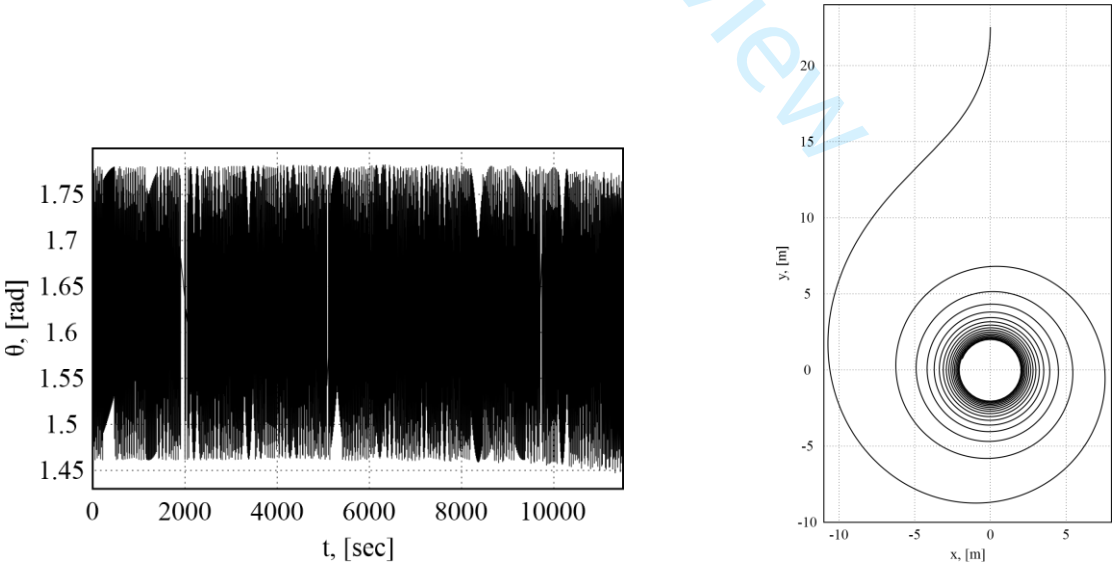

Fig. 13 Time history of the nutation angle $\theta(t)$ and the corresponding trajectory of the E-container $y(x)$ for the initial conditions (60), (62) , the angular spin velocity (61) and for the moments of inertia and mass of the E-container (71).

As follows from Figs. 12 and 13, the reduction of the moments of inertia by half did not lead to a qualitative change in the attitude motion of the E-container. The gravitational and centrifugal (63) and (64) depend on the moments of inertia of the E-container and, in contrast, the electrostatic torque (65) does not depend on the moments of inertia, and Figs. 5, and 13 indirectly confirm that gravitational and centrifugal torques have no appreciable effect on the attitude motion of the E-container near the charged orbiter , which is located at L1 of the libration point.

F. Outer electrically conducting spherical shell of the E-container

As can be seen from Figs. 4, 5, 8 - 13 the E-container performs nutation oscillations within the limits $0, \pi$ and there is no tendency for noticeable damping of oscillations because there are no damping torques in right parts of the equations of attitude motion (54) and (55), which corresponds to the physical essence of the considered process.

And we consider the motion of an E-container having an outer electrically conducting spherical shell. It is obvious that in this case the electrostatic torque is absent. In this case, as follows from Fig. 14 the nutation oscillations retain their initial amplitude as in the base scenario (Fig.5). The reason is the absence of dissipative forces to the damping of nutation oscillations. The numerical simulation are performed or the initial conditions (59) (and (60)), (62) and the angular spin velocity (61).

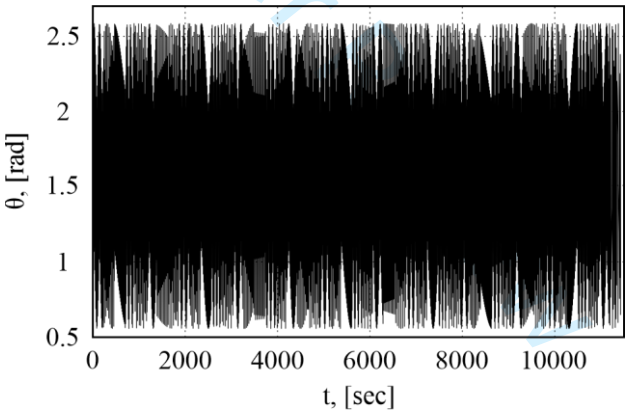

Fig. 14 Time history of the nutation angle $\theta(t)$ of the spherical E-container $y(x)$ for the initial conditions (59), (60) and the angular spin velocity (61).

Now we use the following initial conditions below

$$\theta_0 = 0.01 rad, \dot{\theta}_0 = 0, \psi_0 = 0, \dot{\psi}_0 = 0 \tag{72}$$

and obtain a completely different graph as shown in Fig. 15. That is, the E-container maintains its angular position until it touches the orbiter. The increase in the amplitude at the end of the trajectory can most likely be attributed to an error in the numerical integration.

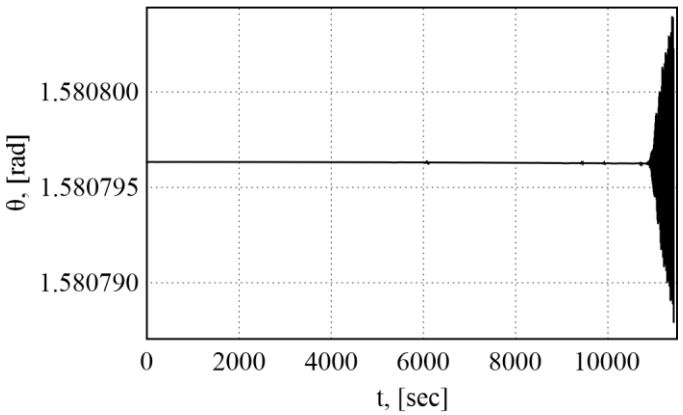

Fig. 14 Time history of the nutation angle $\theta(t)$ of the spherical E-container $y(x)$ for the initial conditions (59), (60) and the angular spin velocity (72).

Comparing the simulation results shown in Figs. 14, 15 with Figs. 4, 5, 8 - 13 come to a quite trivial, that the best solution for is an outer electrically conductive spherical shell of the E-container and the implementation of conditions on the boundary of the Debye sphere of similar (72).

IV.Conclusions

This paper develops the idea of using a potential electrostatic attraction field to capture a small container (Orbit Sample Return) by a large spacecraft (orbiter) when it is necessary to study a center of mass motion of the container in conjunction with an attitude motion if we deal with non-spherical bodies, because at the final phase of capture of this container by the orbiter, it is necessary to know its angular velocity and orientation angles. It may also be noted that this work is a development of the work [13, 14 and 16] on the splitting of collinear libration points by means of a stationary artificial electrostatic field, which now considers the attitude motion in a variable electrostatic field in the vicinity of the L_1 libration point. The new main results of the paper can be briefly summarized as follows:

1) The new equations of the attitude motion of a cylindrical E-container is derived in the Euler angles. These motion equations do not contain terms leading to damping of angular oscillations, which corresponds to the physical nature of the examined motion. In this task, one can only control the voltage level of the orbiter can be controlled, which influences the magnitude of the electrostatic torque acting on the E-container, and does not change the nature of the dependence of this torque on the Euler angles and their derivatives.
2) Study of influence of the initial conditions of the attitude motion and the initial angular spin velocity of cylindrical E-container by means of the numerical integration shows that the reason of large amplitude of oscillation is the electrostatic torque, which cannot be parried by anything. However, in the particular case if,

when entering the Hill sphere, the motion of the E-container was pure precession, in which nutational oscillations are absent, then there was no further excitation of nutational oscillations. Also note that an increase in the initial angular spin velocity leads to a decrease in the amplitude of the nutation oscillations of the cylindrical E-container.

3) Analysis of the simulation results led to the conclusion that the level of voltages insignificantly influences the attitude motion of the E-container. At the same time, it should be taken into account that the greater the product of the orbiter and E-container voltage level, the greater the area of capture of the E-container by the electrostatic field and the Hill sphere with the center in the L1 point libration is larger [14, 15].

4) The influence of gravitational, centrifugal and electrostatic torques is evaluated on the attitude motion of the E-container and recommendations are given on the choice of geometric shape and moments of inertia, which can facilitate a capture of the E-container by the orbiter.

5) The sole solution is to reduce the electrostatic torque to zero, and this is possible if the cylindrical container will be enclosed in a conductive shell or will be shaped like a sphere, and in addition to this it is necessary to implement in a reduction of the amplitude of the nutation oscillations of a cylindrical E-container by means of some devices.

6) The obtained equations of the attitude motion using the Euler angles can be useful both in the classical three body problem and in the problem of docking two charged space objects.

7) The results of this work can be useful not only for the considered particular task, but also for a wider class of spacecraft docking problems on orbits, where due to natural origin static electricity accumulates on the surface of spacecraft.

This paper, along with papers [13, 14, 16], is another step in the study of the possibility of using the E-container to deliver the Phobos Sample Return mission to Earth.

Funding Sources

This study was supported by the Russian Science Foundation (Project No. 19-19-00085).

References

[1] Yoshikawa, Makoto, et al. "The Hayabusa mission." Sample Return Missions. Elsevier, 2021. 123-146. https://doi.org/10.1016/B978-0-12-818330-4.00006-9

[2] Yoshikawa, Makoto, et al. "Hayabusa sample return mission." Asteroids IV 1.397-418 (2015): 1. https://doi.org/10.2458/azu_uapress_9780816532131-ch021.

[3] Watanabe, Sei-ichiro, et al. "Hayabusa2 mission overview." Space Science Reviews 208.1 (2017): 3-16. https://doi.org/10.1007/s11214-017-0377-1

[4] Tsuda, Yuichi, et al. "Hayabusa2–Sample return and kinetic impact mission to near-earth asteroid Ryugu." Acta Astronautica 156 (2019): 387-393. https://doi.org/10.1016/j.actaastro.2018.01.030

[5] Shibata, T., Bennett, T., and Schaub, H., "Prospects of a hybrid magnetic/electrostatic sample container retriever," *Journal of Spacecraft and Rockets*, Vol. 57, No. 3, 2020, pp. 434-445. https://doi.org/10.2514/1.A34509

[6] Lockwood, M. K., "Introduction: Mars Science Laboratory: the next generation of Mars landers," *Journal of Spacecraft and Rockets*, Vol. 43, No. 2, 2006, pp. 257-257. https://doi.org/10.2514/1.20678

[7] Edquist, K. T., Desai, P. N., and Schoenenberger, M., "Aerodynamics for Mars Phoenix entry capsule," *Journal of Spacecraft and Rockets*, Vol. 48, No. 5, 2006, pp. 713-726. https://doi.org/10.2514/1.46219

[8] Gil, P. J. S. and Schwartz, J. "Simulations of Quasi-Satellite Orbits Around Phobos," Journal of Guidance, Control, and Dyrnamics, Vol. 33, No. 3, 2010, pp. 901-914. https://doi.org/10.2514/1.44434

[9] Chen, H., Canalias, E., Hestroffer, D., and Hou, X., Effective Stability of Quasi-Satellite Orbits in the Spatial Problem for Phobos Exploration. *Journal of Guidance, Control, and Dynamics*, Published Online: 9 Aug 2020. https://doi.org/10.2514/1.G004911

[10] Sherwood, B., "Mars Sample Return: Architecture and Mission Design," *Acta Astronautica*, Vol. 53, No. 4-10, 2003, pp. 353–364. https://doi.org/10.1016/S0094-5765(03)00153-X

[11] O'Neil, W., and Cazaux, C., "The Mars Sample Return Project," *Acta Astronautica*, Vol. 47, No. 2-9, 2000, pp. 453–465. https://doi.org/10.1016/S0094-5765(00)00085-0

[12] Dankanich, J., and Klein, E., "Mars Ascent Vehicle Development Status," *IEEE Aerospace Conference*, Big Sky, USA, 2012. https://doi.org/10.1190/AERO.2012.6187295

[13] Aslanov, V. S., "Prospects of Phobos Sample Return Mission Using Electrostatic Container," Journal of Spacecraft and Rockets, 58.6, 2021, 1799-1805. https://doi.org/10.2514/1.A34984

[14] Aslanov, V. S., "Capture Trajectories into Vicinity of Collinear Libration Points by Variable Electrostatic Field," Journal of Spacecraft and Rockets 59.3, 2022, pp. 1039-1043. https://doi.org/10.2514/1.A35250

[15] Nakamura, Tomoki, et al. "Science operation plan of Phobos and Deimos from the MMX spacecraft." Earth, Planets and Space 73.1, 2021, pp. 1-27.

https://doi.org/10.1186/s40623-021-01546-6

[16] Aslanov, V. S., "A Splitting of Collinear Libration Points in Circular Restricted Three-Body Problem by an Artificial Electrostatic Field," Nonlinear Dynamics, Vol. 103, Feb. 2021, pp. 2451–2460.

https://doi.org/10.1007/s11071-021-06226-4

[17] Kane, T. R., and Marsh, E. L., "Attitude stability of a symmetric satellite at the equilibrium points in the restricted three-body problem." Celestial mechanics 4.1 (1971): 78-90.

https://doi.org/10.1007/BF01230323

[18] Robinson, W. J., "The restricted problem of three bodies with rigid dumb-bell satellite." Celestial mechanics 8.2 (1973): 323-330.

https://doi.org/10.1007/BF01231434

[19] Vera, J. A. "On the periodic solutions of a rigid dumbbell satellite placed at L4 of the restricted three body problem." International Journal of Non-Linear Mechanics 51 (2013): 152-156.

https://doi.org/10.1016/j.ijnonlinmec.2013.01.013.

[20] Krasilnikov P. Fast non-resonance rotations of spacecraft in restricted three body problem with magnetic torques //International Journal of Non-Linear Mechanics. 2015c. V. 73. P. 43-50.

http://dx.doi.org/10.1016/j.ijnonlinmec.2014.11.003

[21] Hartzell, C. M., Farrell, W., and Marshall, J., "Shaking as Means to Detach Adhered Regolith for Manned Phobos Exploration," Advances in Space Research, Vol. 62, No. 8, 2018, pp. 2213–2219.

https://doi.org/10.1016/j.asr.2017.09.010

[22] Bechini, M., Quadrelli, M. B., Lavagna, M., andWang, J. J., "Hovering of an Electrically Actuated Spacecraft in a Small-Body Plasma Field," Journal of Spacecraft and Rockets, 2021, pp. 1–16.

https://doi.org/10.2514/1.A34954

[23] Quadrelli, M. B., Garrett, H., Castillo, J., Stoica, A., Ono, M., Christianson, C., Lusso, D., and Schaub, H., "Active Electrostatic Flight for Airless Bodies," 2017 IEEE Aerospace Conference, IEEE Publ., Piscataway, NJ, 2017, pp. 1–16.

https://doi.org/10.1109/AERO.2017.7943821

[24] Stevenson, D., and Schaub, H., "Multi-Sphere Method for Modeling Electrostatic Forces and Torques," Advances in Space Research,Vol. 51, No. 1, Jan. 2013, pp. 10–20.

doi:10.1016/j.asr.2012.08.014

[25] Szebehely, V., Theory of Orbits: The Restricted Three Body Problem, Academic Press, San Diego, CA, 1967.

[26] Schaub,H., and Junkins, J.L., Analytical Mechanics of Space Systems, 2nd ed., AIAA Education Series, AIAA, Reston, VA, Oct. 2009, Chap. 10.

[27] Stevenson, D., and Schaub, H., "Terrestrial testbed for remote coulomb spacecraft rotation control." International Journal of Space Science and Engineering 2.1, 2014, pp. 96-112.

doi: 10.1504/IJSPACESE.2014.060111